1-1-2013

Amplitude vs. Offset Effects on Gas Hydrates at Woolsey Mound, Gulf of Mexico

Walter R. Anderson
University of South Carolina

Amplitude vs. Offset Effects on Gas Hydrates at Woolsey Mound, Gulf of Mexico

by

Walter R. Anderson Jr.

Bachelor of Science

University of South Carolina, 2010

Submitted in Partial Fulfillment of the Requirements

For the Degree of Master of Science in

Geological Sciences

College of Arts and Sciences

University of South Carolina

2013

Accepted by:

Camelia C. Knapp, Major Professor

James H. Knapp, Reader

James N. Kellogg, Reader

Lacy Ford, Vice Provost and Dean of Graduate Studies

Dedication

This work is dedicated to my loving parents, who have never once believed that I wasn't capable of anything and everything I've dreamed of accomplishing, and to my family and friends, who have kept me going through 20 years of education.

Acknowledgments

We would like to acknowledge the Gulf of Mexico Hydrate Research Consortium (GMHRC) and TGS-Nopec for obtaining and providing data used in this study. Thanks to the U.S. Department of Energy and Minerals Management Service for funding this research. Special thanks go to Geophysical Exploration and the Tectonics and Geophysics Laboratories (GEL and TGL) from the Department of Earth and Ocean Sciences at the University of South Carolina. We would also like to acknowledge Landmark Graphics Corporation and Veritas Hampson-Russell for the use of their software (ProMAX and AVO).

Abstract

Due to the estimated massive quantities of natural methane hydrates, they represent one of the largest sources of future alternative energy on Earth. Methane hydrates have been found in the shallow sub-seafloor of the Northern Gulf of Mexico where the water depth is in excess of ~900 m. Mississippi Canyon Block 118 has been chosen by the Gulf of Mexico Hydrates Research Consortium to be the site of a multi-sensor, multi-discipline sea-floor observatory for gas hydrate research. First evidence for gas hydrates at MC 118 was observed at Woolsey Mound. Subsurface evidence for gas hydrates has subsequently been substantiated by 3D seismic reflection data and piston coring. It is estimated that methane trapped within gas hydrates worldwide may exceed 10^{16} kg, one of the largest sources of hydrocarbons to date, and here they present an opportunity for exploitation via harvesting for energy production. The analysis of the 3-D seismic reflection data and integration with industry well logs reveals the subsurface structural and stratigraphic architecture of a thermogenic hydrate system in the Mississippi Canyon area (MC-118) of the Gulf of Mexico. Like many hydrocarbon systems in the Gulf of Mexico, Woolsey Mound is dominated by the presence and sporadic movement of allochthonous salt within the sedimentary section. Exploration-scale 3-D seismic imaging shows a network of faults connecting the mound to a salt diapir and an extended area of high P-wave velocity just beneath the sea floor. Gas hydrates exhibit clear seismic properties such as the bottom simulating reflector (BSR), relatively high P- and S- wave velocities, seismic blanking, and

amplitude vs. offset (AVO) effects. These effects occur mainly due to the presence of free gas that is usually trapped by the more rigid overlying hydrate formations. In order to substantiate the presence of hydrates in the shallow subsurface at Woolsey Mound, an AVO analysis based on the variation of the P-wave reflection coefficient with the angle of incidence was performed on a seismic transect across the mound. The AVO analysis targeted a shallow (~150 m below the seafloor) "bright spot" that is interpreted to mark the base of the gas hydrate stability field. The AVO analysis shows results consistent with evidence for free gas underlying a medium with higher P-wave and S-wave velocities such as gas hydrates. This shallow, high-velocity zone, pore-fluid analyses revealing microbial processes, thermobaric and AVO analysis provide convincing evidence for the existence of gas hydrates at MC 118.

Table of Contents

I. Introduction

Clathrate hydrates are crystalline hydrogen compounds in which guest atoms or molecules are physically trapped within the three dimensional structure. These compounds are known as gas hydrates when the enclosed molecules are gases (Chatti et al 2005). Light gases such as methane and ethane are extremely common within these compounds, as their molecular structures fit well with that of the icy barrier. The water and gas molecules are so closely intertwined that their interactions actually help to stabilize the structure. A significant fraction of the icy cavities must be occupied with gas molecules to ensure stability (Buffett, 2000).

Hydrates possess a profound ability to store large volumes of gas. This defining characteristic leads to the primary interest in gas hydrates, and unprecedented volumes of hydrate are expected to exist in many locations across the planet. It is estimated that global stores of methane trapped within marine hydrate may exceed 2×10^{16} kg, one of the largest sources of hydrocarbon on Earth (Buffet 2000). This capacity for storage and stability can also be used in marine carbon dioxide sequestration and natural gas storage and transportation (Chatti et al., 2005).

However, interest in clathrate hydrates also stems from the dangers they present to petroleum exploration and recovery programs, primarily through drilling hazards and pipeline plugs. Hydrate can act as a lubricating layer within sediments and lead to slumping on the continental slope and can dissociate quickly when drilled, leading to mud volcanoes and explosions (Diaconescu and Knapp 2002). Another primary concern is the radiative properties of methane, a powerful greenhouse gas, in the atmosphere. There has not yet been a clear relation between the release of large volumes of methane trapped in hydrates and global climate change, but the concept is simple to understand. Small changes in sea temperature or pressure and slumping in the continental margins are favorable situations for the dissociation of the gas hydrates (Buffett 2000).

Thus, it becomes necessary to find effective and relatively inexpensive methods to locate gas hydrates in the Earth's continental margins. An analysis of the variation in the amplitudes of seismic waves with a change in the angle of offset, or amplitude

versus offset (AVO) analysis, is an example of a method which accomplishes this. An AVO analysis provides an accurate method to locate gas hydrates without the need to drill. AVO has been used by the petroleum industry in the last two decades in order to determine rock's fluid content, porosity, density or seismic velocity. AVO refers to the dependency of the seismic amplitude with the distance between the source and receiver (the offset) and is based on the relationship between the reflection coefficient and the angle of incidence based on the Zoeppritz equations. Since gas hydrates can act as seals to trap hydrocarbon gases in marine sediments, the AVO analysis has also been used as an indicator of the base of the gas hydrate stability zone. Therefore, in this paper, we will show that the bottom of the hydrate stability zone (HSZ) within Mississippi Canyon lease block 118 (MC-118) at Woolsey Mound can be located with the use of 2-D seismic reflection data and an AVO analysis of interpreted "bright" reflectors in the shallow sub-seafloor.

II. Geologic Setting

Woolsey Mound, a carbonate/hydrate mound approximately one kilometer in diameter, is located in the southern portion of Mississippi Canyon lease block 118 (MC-118). MC-118 is located offshore approximately 150 km south of Pascagoula (Ms) and 100 km east of the Mississippi Canyon, ~890 m below sea level (Figure 1). It sits on the eastern flank of the main Mississippi Canyon, in a gently seaward dipping portion of the continental slope. On the Gulf's continental slope, faults and fractures radiating from salt bodies produce natural conduits that facilitate migration of hydrocarbon fluids from deeper oil reservoirs into the Hydrate Stability Zone (HSZ) (Simonetti et al., *in press*). The supply of hydrocarbons (natural gas and petroleum) to the seafloor supports active biological seep communities and microbial chemolithotrophy in the vicinity of active gas-fluid seepage (Lapham et al., 2008). Visible outcrops of hydrates, faulted carbonates and pockmark features, cover approximately 1 km^2 of the seafloor. The seaward slope across the area ranges from 3^o to 4^o, but steeper 10^o-12^o are present locally across the pockmark (Macelloni et al., 2012).

Like many hydrocarbon systems in the Gulf of Mexico, MC-118 is dominated by the presence and sporadic movement of allocthonous salt within the sedimentary section. The northwestern flank of the salt body appears to reach depths suitable for hydrocarbon maturation, while the steeper flanks provide migration pathways for deep basin fluid flow. A radiating crestal fault structure above the salt creates delivery systems to the shallower subsurface as well as venting at the seafloor (Figure 2).

Stratigraphic relationships indicate that the most recent period of salt movement was probably during the Late Pliocene. Subsequently, the Pleistocene time was characterized by relatively uniform, quiescent sedimentation over the mound site. Such relationships suggest that the gas hydrate system at MC-118 is likely a geologically young feature (Knapp et al., 2010).

III. Hydrate Stability

Theoretically-determined phase equilibria can be used to calculate temperatures and pressures at which hydrates are stable for a given gas composition, and clearly distinguish natural gas hydrates from water ice (Sloan 1998). Phase equilibrium diagrams developed to calculate the stability conditions of gas hydrates given certain conditions of temperature, pressure, and gas composition are defined by requiring the clathrate phase to coexist with both the liquid and vapor phases in a three-phase equilibrium as shown in Figure 3 (Buffett, 2000; Sloan., 1998; Trehu et al., 2006). This state of equilibrium occurs at a certain temperature which is solely a function of pressure P (red curve in Figure 3). A hydrostatic pore-pressure gradient of 0.1 atm/m was assumed for calculating the depth scale. In such a diagram, gas hydrate is stable to the left side of the red curve. Since gas hydrates are stable at low temperatures and high pressures, their formation is limited to either polar regions under permafrost or cooler marine continental slopes where water depths typically exceed ~400-500 m (e.g. Diaconescu et al., 2001). Pure methane hydrates are less stable than hydrates composed of methane plus heavier hydrocarbon gases such as ethane, propane, butane, etc. Furthermore, inclusion of CO_2 or H_2S would increase the hydrate stability whereas salinity and N_2 would make the hydrates less stable. In seabottom sediments, the upper limit of the hydrate stability zone (GHSZ) is marked by the intersection of the hydrate stability curve with the seafloor isotherm. The bottom of the GHSZ is marked by the intersection of the hydrate stability curve with the geothermal gradient (Fig. 3b). Therefore, knowledge of the temperature and pressure fields together with the hydrocarbon gas composition and ocean water salinity are critical parameters in estimating and predicting the gas hydrate formation conditions.

The hydrate stability field at Woolsey Mound was calculated based on the thermogenic gas composition sampled at the site (Lapham et al., 2008) and a geothermal gradient of ~17°C/km derived from the ARCO-1 and associated ARCO-2 sidetrack wells (Fig. 4b). Two industry wells (ARCO-1 and ARCO-2) were drilled in 1989. These wells tested the interval down to 1864 and 2762 mbsf respectively, and are located ~580 m NW of the hydrate-

carbonate mound. Preliminary analysis of the temperature data from the wells predicts a very thick (~1.2 km) hydrate stability zone at the well locality (Fig. 4a). However, the geophysical signature above the hydrate mound suggests a much thinner and shallower hydrate stability field, consistent with the inferred higher temperatures and salinities expected above the SW salt body. Based on the 3D seismic volume, we interpret shallow bright spots that we assume to be Bottom Simulator Reflectors (BSR) to mark the base of the gas hydrate stability field, at ~ 150 mbsf. Thermobaric modeling of the stability field from this constraint suggests much higher geothermal gradients on the mound (Fig. 4b).

Of the different equations developed for gas hydrate phase-equilibria, we employed the three-phase equilibrium analysis based on a statistical thermodynamic determination of the distribution of the guest particles in the hydrate structure (Van der Waals and Platteeuw, 1959; Sloan, 1990). This approach provides a comprehensive means of correlation and prediction of all the hydrate equilibrium regions of the phase diagram, without separate prediction schemes for two-phase regions, three-phase regions, etc. (Sloan, 1998). The intersection of the gas hydrate stability curve (in red in Fig. 4) with the seafloor isotherm of 4.85^{o}C denotes the minimum water depth at which gas hydrates are stable for a given hydrocarbon gas composition (Fig. 4b). The depth at which the geothermal gradient intersects the gas hydrate stability curve marks the predicted base of the gas hydrate stability field (Kvenvolden et al., 1981; Kvenvolden, 1993a, b). Based on this thermobaric modeling, the geothermal gradient derived to match the shallow bright spots is ~115°C/km, much higher than that derived from the temperature measurements in the ARCO well. This significant temperature variation in the sediments between the hydrate mound and the outside area may be due to the high flux of thermogenic gas migrating upwards in the vicinity of the shallow faults. Therefore, a better knowledge of the temperature and pressure conditions is critical for an accurate prediction of the GHSZ at the Woolsey Mound.

IV. The Bottom Simulating Reflector (BSR)

The seismic reflection technique is currently recognized as the primary tool used for the inference of natural gas hydrates within marine sediments. The preliminary feature indicative of the presence of gas hydrates is a strong bottom simulating reflector (BSR), a negative polarity reflector which mimics the topography of the seafloor (Diaconescu et al, 2001; Figure 5). Satyavani et al. (2003) have proposed two methods for the formation of the BSR. In the first, the presence of gas hydrates within the sediments

causes a sharp increase in the P-wave velocity, generating a strong reflector associated with the top of the HSZ. In the second, the strong reflector is caused by hydrates overlying gas-saturated sediments. In this situation, the high impedance contrast results from the interface between the overlying sediments containing hydrate and the underlying gas-saturated sediments having lower velocity, slightly lower density and, consequently, signals the bottom of the HSZ. The BSR typically follows the subsurface isotherm approximately parallel to the sea-floor and cuts across layered sediments. Therefore, the BSR is a phase boundary or a thermobaric boundary between gas hydrate charged sediments above and free gas charged sediments below it. However, a lithologic boundary with a distinct impedance contrast can also create an appearance similar to the BSR, thus it becomes important to use precaution when interpreting such sections and the need to use other methods to locate the HSZ are required.

V. Amplitude Variation with Offset

The variation of reflection and transmission coefficients with the incident angle is referred to as offset-dependent reflectivity and is the basis for seismic AVO analysis (Castagna, 1993). The variations are shown with the Knott (1899) and Zoeppritz (1919) equations, which are unmanageable and complex in form. Shuey (1985) presented an approximation of the equations which greatly simplifies AVO interpretation with:

$$R_{PP}(\theta_1) \cong R_P + \left(A_0 R_P + \frac{\Delta\sigma}{(1-\sigma)^2}\right)\sin^2\theta_1 + \frac{1}{2}\,\frac{\Delta V_P}{V_{P\alpha}(\tan^2\theta_1 - \sin^2\theta_1)} \quad (1)$$

Where,

$R_{PP}(\theta_1) =$ P-wave reflection coefficient as a function of incident angle, θ_1,

$R_P =$ normal incidence reflection coefficient,

$A_0 = B_0 - 2(1 + B_0)\left(\frac{1-2\sigma}{1-\sigma}\right)$,

and $B_0 = \frac{\frac{\Delta V_P}{V_{P\alpha}}}{\frac{\Delta V_P}{\Delta V_{P\alpha}} + \frac{\Delta\rho}{\Delta\rho\alpha}}$.

The first term is the normal incidence reflection coefficient, the second term predominates at intermediate angles, and the third term is dominant as the critical

angle is approached. Thus, for restricted angles of incidence, equation (1) is linear in $\sin^2 \theta_1$.

$$R_{PP}(\theta_1) \cong R_P + B \sin^2 \theta_1 \quad (2)$$

Here we use "*A*" to represent the normal incidence reflection coefficient R_P, or the "AVO intercept". *B* is called the "AVO gradient" and is shown by Wiggens et al. (1983) to be:

$$B = R_P - 2R_S. \quad (3)$$

AVO analysis for nonbright-spot reflectors is facilitated by cross-plotting extracted seismic parameters of AVO intercept (*A*) and gradient (*B*). Focused cross-plots for these two AVO parameters create charts on the *x* and *y* coordinate plane, where *A* is the horizontal axis and *B* is the vertical axis. A typical AVO response will plot in one of three quadrants, each representing a particular arrangement within the subsurface:

1) If the reflection coefficient increases with offset across the interface, the majority of points in the cross-plot should appear in quadrant IV;
2) If the reflection coefficient decreases with offset across the interface, and the overlying medium is shale, then the majority of the points will appear in quadrant III; and
3) If the reflection coefficient decreases with offset across the interface, and the overlying medium is hydrate, then the majority of the points will appear in quadrant II.

The distinguishing factor between points 2 and 3 is shear wave velocity, V_s, which is lower in shales than in hydrates.

Furthermore, in the absence of hydrocarbon bearing strata, this cross-plot often forms a well-defined "background trend." (Figure 6) Thus, deviation from this trend can be viewed as an indicator of the presence of hydrocarbons (Castagna et al., 1998).

Seismic reflections from gas bearing sands exhibit a wide range of amplitude versus offset (AVO) characteristics (Figure 7). These variations have classically been separated into three classes, which are based most strongly on two factors: 1) the normal incidence reflection coefficient R_0 and 2) the contrast in Poisson's ratio at the reflector:

Class I – High-impedance sands,

Class II – Near-zero impedance contrast sands, and

Class III – Low-impedance sands (Rutherford and Williams, 1989).

Class I gas sands display a reflection coefficient which decreases with increasing offset, Class II gas sands display a reflection coefficient which may increase or decrease with offset and may reverse polarity, and Class III gas sands tend to have an increased reflection coefficient with offset, which are illustrated in figure 7.

More recently, Castagna et al. (1998) hypothesized the existence of a fourth type, Class IV, which has an impedance contrast lower than that of the overlying unit, but has a reflection coefficient that decreases in magnitude with offset. Class IV gas sands typically occur when porous sand is overlain by a high-velocity unit, such as a hard shale, siltstone, tight sand, or gas hydrate and can be used as evidence for the bottom of the hydrate stability zone, where free gas collects in the porous sediments underlying gas hydrate.

VI. Methods

In order to constrain the location of BSR at Woolsey Mound, we have processed and interpreted seismic reflection data from MC-118 (provided by TGS-Nopec Geophysical Company) using ProMAX software in order to locate the BSR, salt diapir(s), fault structures and bright, shallow reflectors associated with hydrate presence.

Data was collected using four streamers at a length of 7200 m, with a line length of ~10 km. This line crosses directly over the ~1.5 km^2 Woolsey Mound (Figure 2). The shotpoint interval is 31.25 m with a receiver spacing of 25 m and a record length of 12.288 s. For the purposes of this research, only the top 3 s of the seismic data are used. Data processing steps include bandpass filtering, velocity analysis, normal moveout correction, CDP stacking and a slight static correction. The AVO analysis requires the preservation of the true reflection amplitudes and, therefore, uses pre-stacked data. Acquisition and processing parameters used in this study are shown in Tables 1 and 2, respectively.

Shallow bright reflectors in the resulting interpreted seismic image (Figure 5) have been targeted for the AVO analysis. Increasing or decreasing amplitude with offset within the CDP gathers has been shown by Castagna et al. (1998) and Satyavani et al. (2003) to be an indicator of hydrocarbon presence.

VII. Discussion

Gas hydrates exist within MC-118 as outcrops on the sea-floor and in the shallow sub-seafloor as seen in piston cores acquired by the University of Mississippi (Simonetti et al., in press). However, in order to gain a more definitive location for the boundaries of the hydrate stability zone, AVO analysis was conducted using seismic reflection data provided by TGS Nopec Geophysical Company and software provided by Hampson-Russell.

The faults illustrated in the section are conduits along which hydrocarbons flow into the shallow sub-surface, where they enter into the hydrate stability zone. Thus, AVO analysis was performed along shallow reflectors above and to either side of the salt dome. Conclusive results indicating the bottom of the HSZ were found along the first bright reflector, ~150 ms beneath the sea-floor and highlighted blue in figure 5.

Along this targeted shallow reflector, an AVO analysis using small groups of common depth points (CDPs) indicates that the reflector is coincident with a sharp decrease in the P-wave velocity across the interface (Figure 8). Furthermore, it is shown that the overlying high velocity interface also presents a high shear velocity (V_s) by plotting in quadrant II of the AVO cross-plots.

Directly above the salt dome, between approximately CDPs 400-440, the AVO response curve indicates a decrease in the impedance contrast along the reflector at ~150 ms, but has a reflection coefficient that decreases in magnitude with offset. This pattern is repeated both to the North and South of the salt dome along the line, between approximately CDPs 320-375 and CDPs 450-515 (Figure 8). It is important to note that in each of the cross-plots shown in figure 8, many of the data points plot in quadrant II, below the background trend line, a strong indicator for the presence of free gas within the underlying sediments. We interpret this pattern as the hydrate of Woolsey Mound acting as a seal for free gas moving upward through the fault system.

Figure 10 shows an AVO response expected of typical ocean floor sediments, with a velocity that increases with depth. This control example shows the cross-plot and curve

between CDPs 850-875, ~5 km North of Woolsey Mound, where no interpreted faults are thought to be supplying hydrocarbon fluids to the HSZ.

VIII. Conclusions

The seismic acquisition parameters and processing steps have yielded the interpreted Line A shown in figure 5, which illustrates several shallow bright reflectors, the salt diapir, normal faulting and BSR from AVO analysis. It is important to note that very little processing is used during the AVO analysis, in order to preserve the true reflection amplitudes and the "blanking" effects of hydrate.

The ARCO wells have shown a geothermal gradient of 17^{o}C/km at ~580 m NW of Woolsey Mound. This gradient would produce a HSZ down to ~1200 m under normal conditions, but the extreme proximity of the salt diapir vastly increases subsurface salinity and temperature, destabilizing the hydrate and shallowing the HSZ. Furthermore, we have shown that the BSR at ~150 mbsf exhibits AVO signals associated with the bottom of the HSZ. Between CDPs 320 and 515, the analysis shows a sharp decrease in P-wave velocity as well as a decreasing reflection coefficient with an increasing angle of offset across the blue reflector above the salt diapir. These findings indicate a shallow HSZ and a relatively higher geothermal gradient through Woolsey Mound.

In conclusion, it is demonstrated that location of the BSR associated with the bottom of the HSZ can be located at Woolsey Mound of MC-118 using an AVO analysis method. At Woolsey Mound, hydrocarbon fluids move up into the shallow sub-surface and into the HSZ, where pressure and temperature conditions allow for the formation of methane hydrate. At the bottom, this hydrate acts as a seal for free gas. The lower bounds of the HSZ, based on the AVO readings, are shown in figure 8. A major strength of this research lies in that the AVO analysis was completed without the use of well log data, thereby eliminating the need for expensive drilling to locate possible zones of hydrate accumulation.

IX. Figures

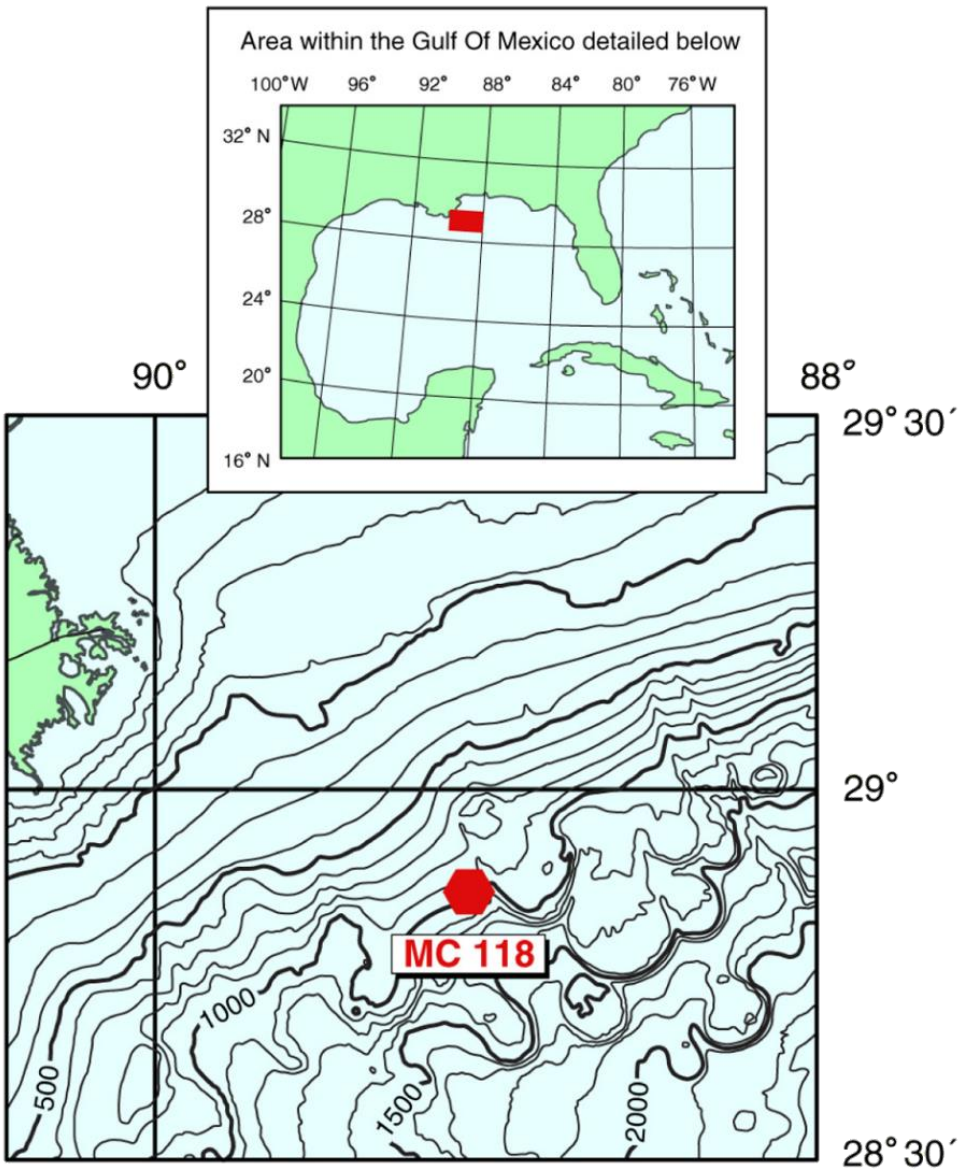

***Figure 1**: Location of MC-118 within the Gulf of Mexico. It lies on the eastern flank of the Mississippi Canyon approximately 890 m below sea level (after McGee et al., 2009).*

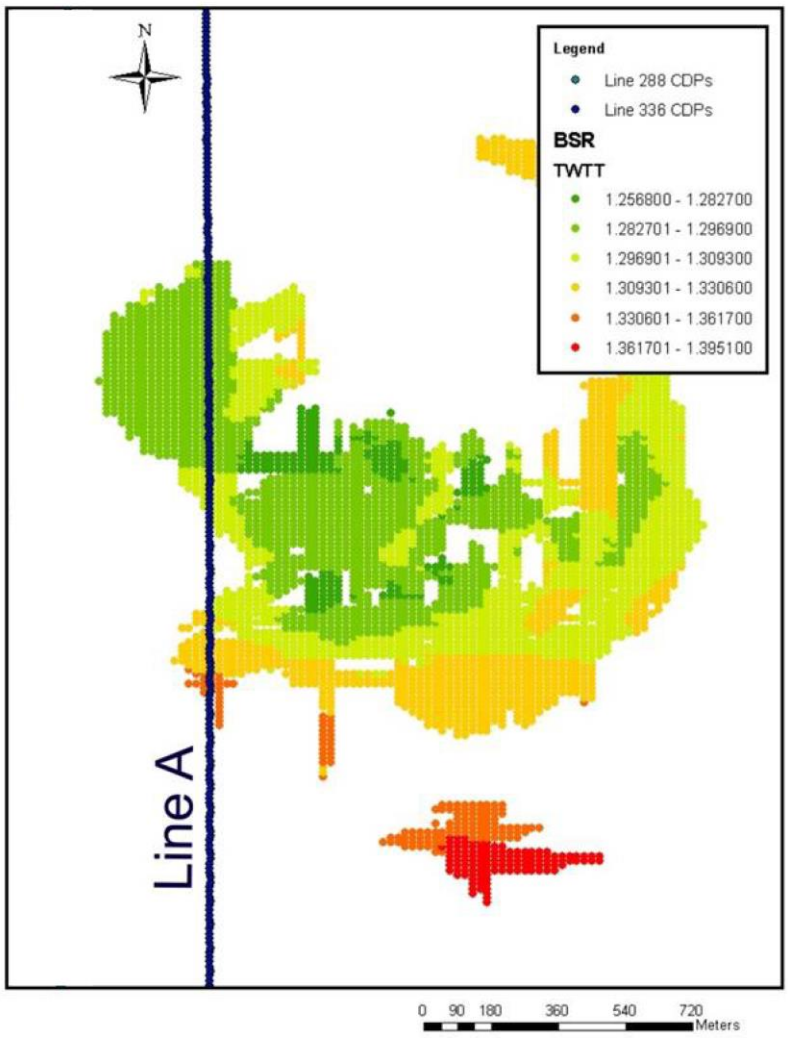

Figure 2: Location map of two survey lines through MC-118. For this research, Line A has been processed and interpreted in Figures 3 and 4. Green to yellow to red colors represents two-way travel time (TWTT) contours of the mapped shallow "bright spots" inferred as bottom simulating reflectors (BSRs).

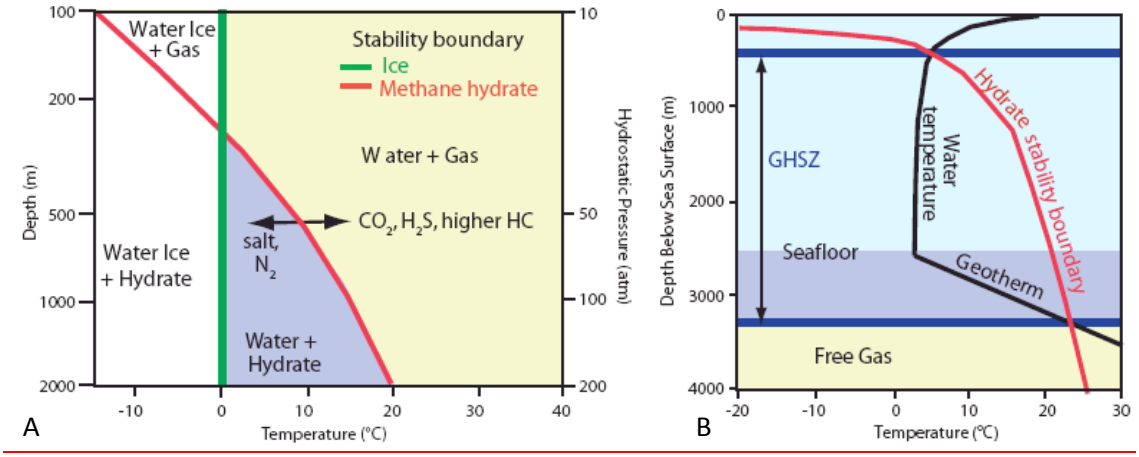

Figure 3: (A) Methane hydrate stability curve as compared to water ice (salinity is considered negligible). Methane hydrate becomes more stable if gas contains CO2, H2S, or higher-order hydrocarbons, and less stable if pore-water salinity increases or if the gas contains N2. (B) Gas hydrate phase equilibrium diagram showing hydrate stability in the ocean. Red curve shows the gas hydrate stability boundary. The gas hydrate stability zone (GHSZ) is marked by the intersection of the hydrate stability boundary with the seafloor isotherm at the top, and the intersection with the geothermal gradient, at the bottom. The thickness of the GHSZ below the seafloor increases as water depth increases given that the geothermal gradient stays constant (after Trehu et al., 2006).

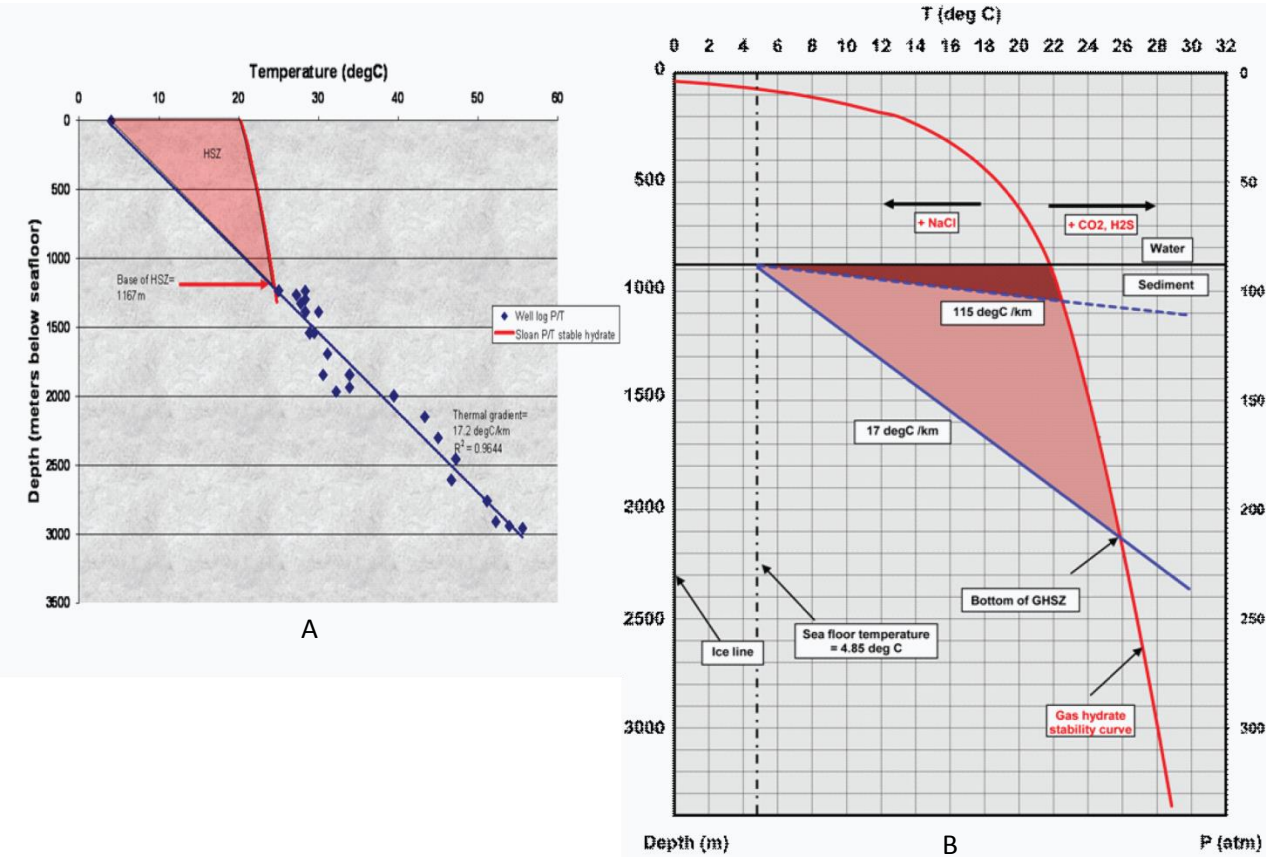

Figure 4: (A) Predicted base (~1200 mbsf) of the GHSZ (gas hydrate stability zone) in the vicinity of the MC-118 ARCO-1,2 wells based on temperature data from the wells using CSMHYD model (after Lapham, pers. Comm..). (B) Phase equilibrium diagram for the gas hydrate system at MC-118 taking into account seafloor depth of ~890 m and seafloor temperature of 4.85°C. Assumptions include normal seawater salinities (3.5% salts), and thermogenic gas composition (70% methane, 8% ethane, 16% propane, and 6% n-butane, reported in Sassen et al., 2006). The shallow bright spots (~150 mbsf) on the mound imply a much shallower GHSZ above the SW salt dome (from lighter to darker red). Depth scale assumes a pore-water hydrostatic pressure gradient of 0.1 atm/m.

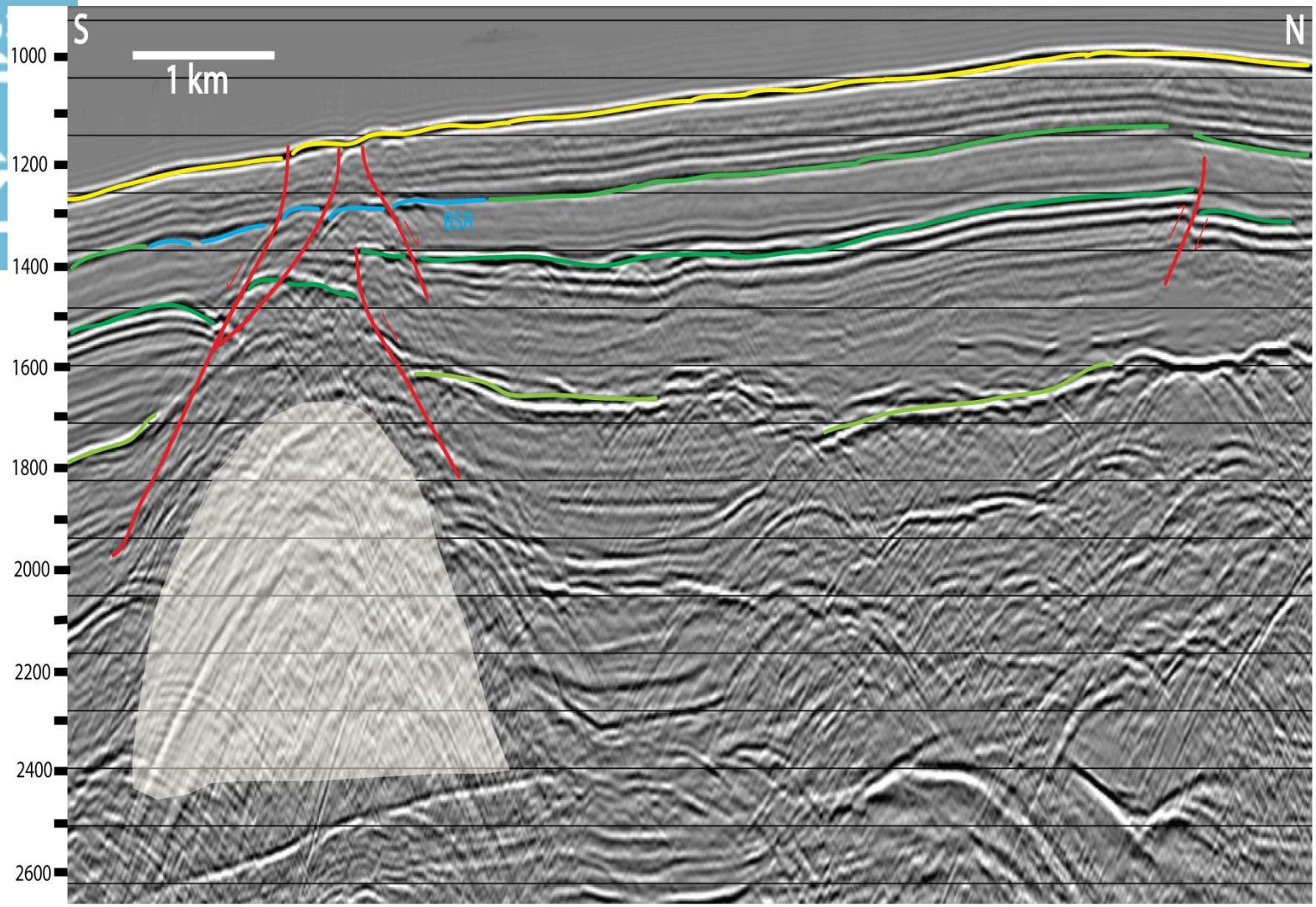

***Figure 5**: Processed, interpreted two-way travel time (TWTT) seismic section at MC-118 showing seafloor in yellow, allocthonous salt in white, faults in red and bright reflectors in green. The BSR associated with the bottom of the hydrate stability zone (HSZ) is shown in blue.*

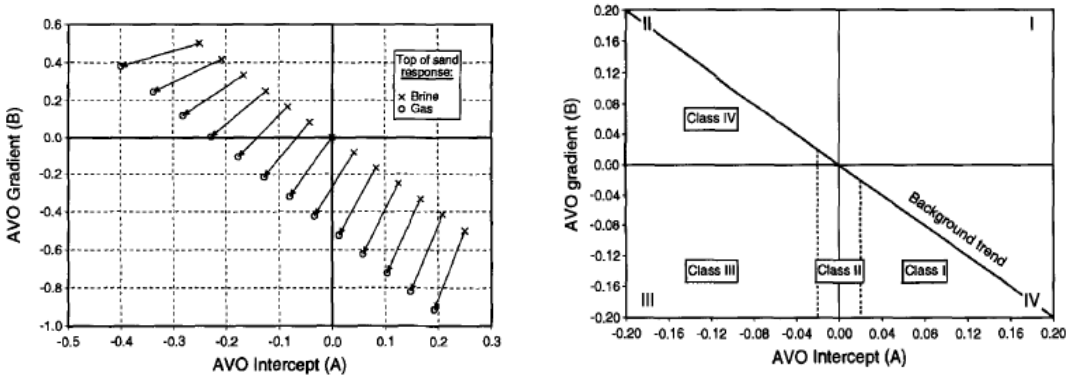

***Figure 6**: Left – the movement of AVO reflection coefficients from the background trend as gas replaces brine within a sandy layer below shale. Right – AVO intercept (A) vs. gradient (B) crossplot showing four possible quadrants. Brine-sands tend to fall along the background trend line, while Class I-IV gas-sands fall in their designated areas.*

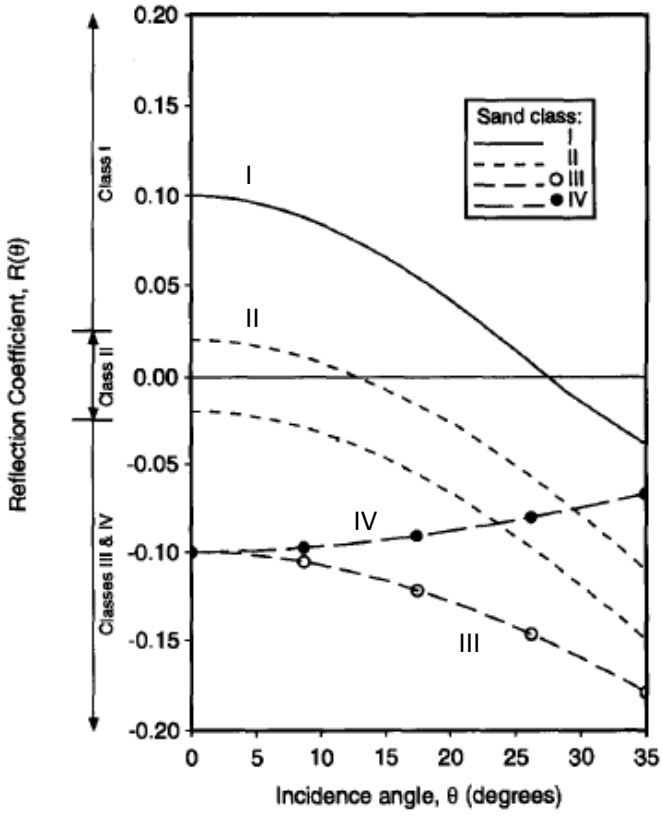

***Figure 7**: For Class I, II, and III gas sands, reflection coefficients tend to decrease with an increasing angle of offset. This differs from Class IV, which displays an increasing reflection coefficient with offset, but a decreasing amplitude magnitude.*

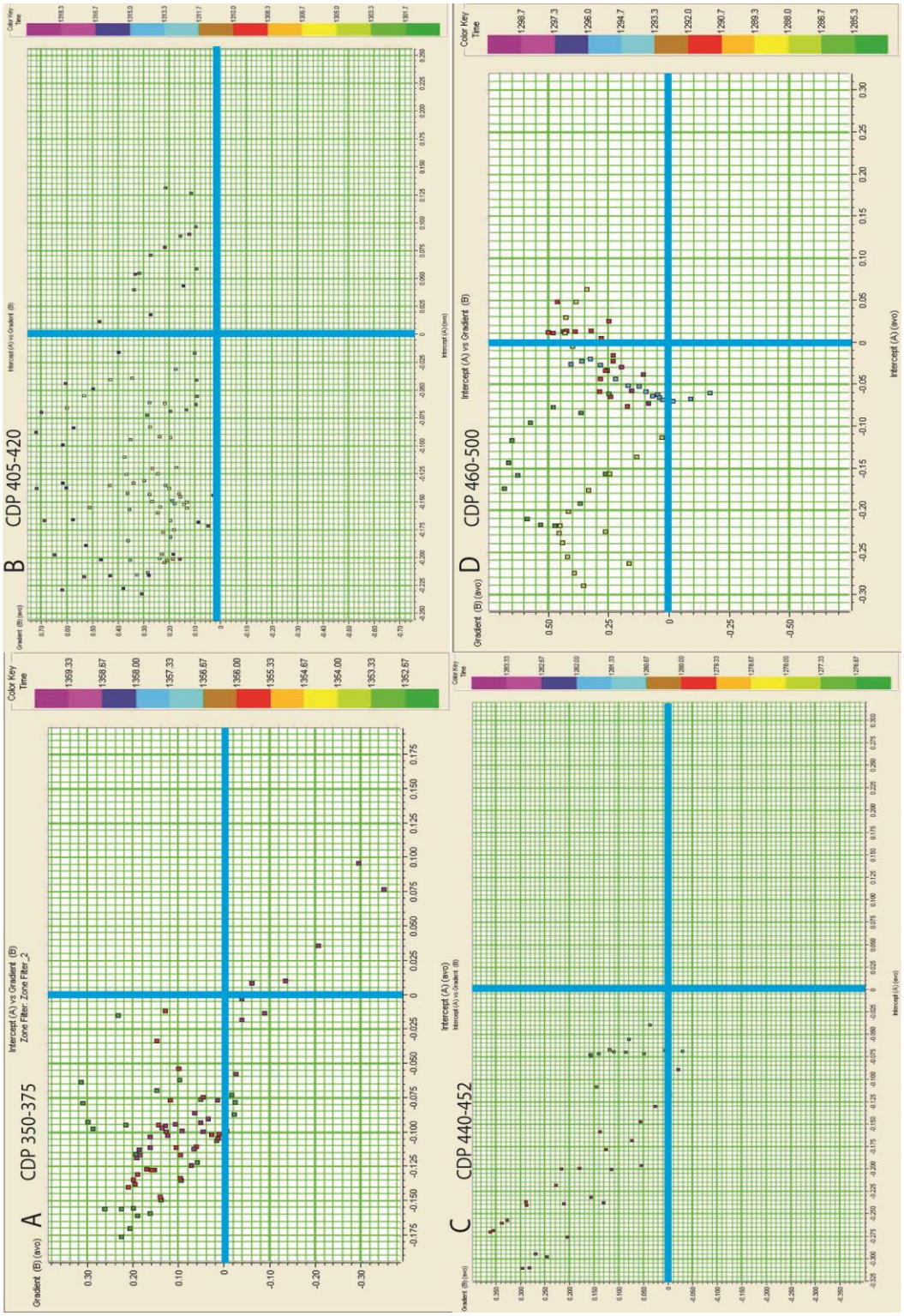

***Figure 8**: AVO cross-plots showing a strong majority of points within quadrant II, indicating a decrease in reflection coefficient with increasing offset across the interface. The cross-plots occur*

along the reflector marked "BSR" in figure 5. Plot A shows CDPs 350-375, south of the salt dome. Plots B and C show CDPs 405-420 and 440-452, directly above the salt dome. Plot D shows CDPs 460-500, to the north of the salt dome.

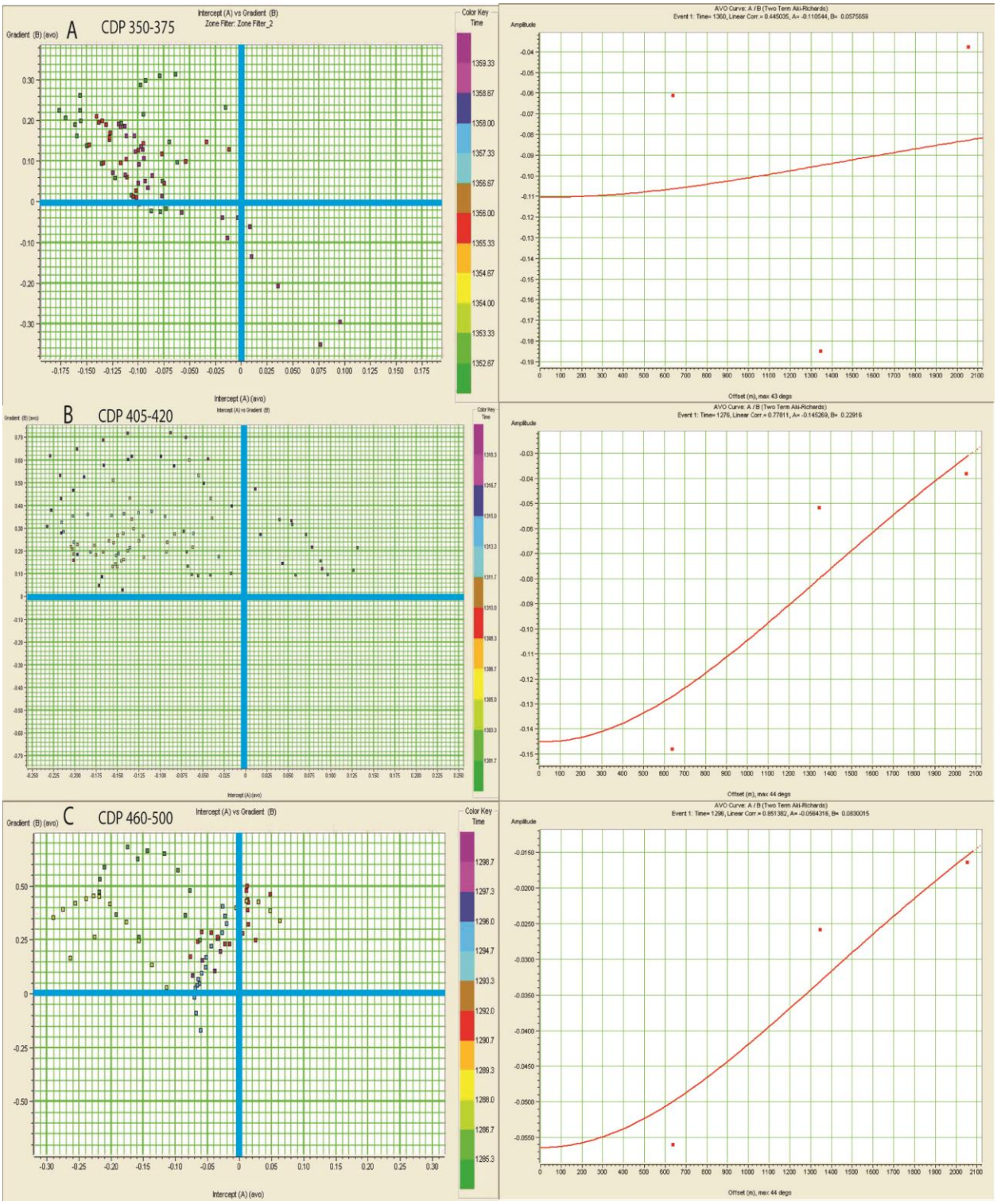

***Figure 9**: Cross-plots and their associated gradient curves. Each curve shows the Class IV AVO response of decreasing absolute value of the amplitude with increased offset, indicative of free gas beneath a high velocity layer, in this case,*

gas hydrate. Plots A, B and C each represent positions to the South, directly above and North of the salt dome, respectively, and correspond to their curves to the right.

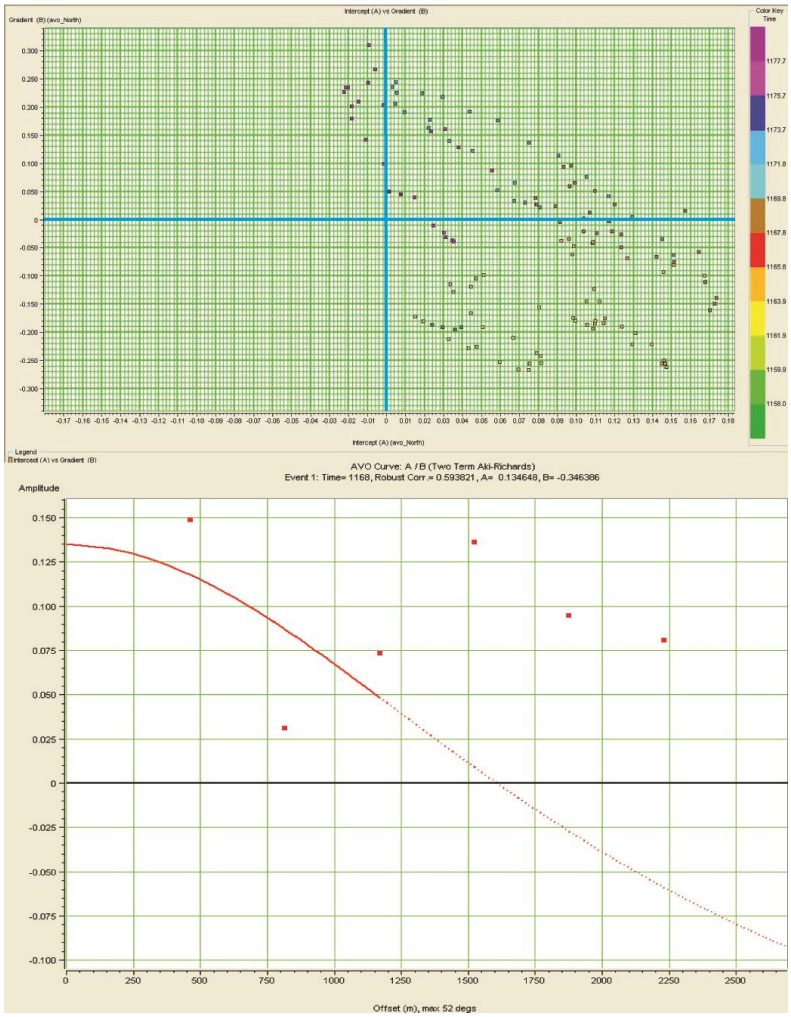

Figure 10: *The AVO cross-plot for CDPs 850-875 (top) shows a normal AVO response at an interface separating a lower velocity overlying medium from a higher velocity underlying medium in the absence of hydrocarbons. These CDPs are ~5 km North of Woolsey Mound, where no interpreted faults are thought to be supplying hydrocarbon fluids to the shallow subsurface. The corresponding AVO curve (bottom) shows the Class I response expected from this positive reflection coefficient interface.*

X. Tables

Streamers	*4 per line*
Airgun Source	*4180 in^3*
Line Length	*~10 km*
Shotpoint interval	*31.25 m*
Record length	*12.288 s*
Receiver spacing	*25 m*
Streamer length	*7200 m*
Sample rate	*2 ms (desampled to 4 ms)*
Channels	*288*

Table 1: *Acquisition parameters used by TGS-Nopec Geophysical Company.*

Geometry
Spherical divergence correction
Spiking/predictive deconvolution
Bandpass filter (4-8-60-70 Hz)
F-X decon (shot domain)
Static correction (-128 ms)
Velocity Analysis
Normal Moveout Correction
F-K filter (multiple suppression)
CDP median stack
Coherency filter
Finite Difference migration

Table 2: *Example processing flow used to optimize the appearance of the hydrate seismic characteristics.*

XI. References

Buffett, Bruce A., 2000. "Clathrate Hydrates". Annual Reviews of Earth and Planetary Sciences 28:477-507. Department of Earth and Ocean Sciences, University of British Columbia. Vancouver, Canada.

Castagna, John P., 1993. "AVO Analysis – Tutorial and Review" ARCO Oil and Gas Company, La Palma, California.

Castagna, John P., H. W. Swan, and D. J. Foster, 1998. "Framework for AVO gradient and intercept interpretation." *Geophysics*, Vol. 63, No. 3 (May-June 1998); P. 948-956.

Chatti, I., Delahaye, A., Fournaison, L., Petitet, J., 2005. "Benefits and Drawbacks of Clathrate Hydrates: a Review of Their Areas of Interest". Energy Conversion and Management 46 (2005), 1333-1343.

Diaconescu, C. C., Kieckhefer, R. M., and J.H. Knapp, 2001. Geophysical Evidence for and Thermobaric Modeling of Gas Hydrates in the Deep Water of the South Caspian Sea, Azerbaijan, *Marine and Petroleum Geology*, 18, 209-221.

Knapp, C. C., J. H. Knapp, D. Terry, 2010. "Geological and Geophysical Baseline Characterization of Gas Hydrates at MC118, Gulf of Mexico." Department of Earth and Ocean Sciences, University of South Carolina. Columbia, SC

Knapp, J. H., C. C. Knapp, L. Macelloni, B. Battista, 2009. "Climate Hazard or Future Energy Resource?: Subsurface Architecture of a Dynamic Hydrate System in the Gulf of Mexico." Department of Geological Sciences, University of South Carolina.

Kvenvolden, K. A., 1993. "A Primer on gas hydrates, in The Future of Energy Gases", U. S. Geological Survey professional paper 1570, a, 279.

Kvenvolden, K. A., 1993. Gas hydrates as a potential energy resource –a review of their methane content. In The Future of Energy Gases (eds Howell, D. G. et al.), US Geological Survey Professional Paper, b, vol. 1570, pp. 555–561.

Kvenvolden, K. A., Barnard, L.A., Brooks, J.M. and Wiesenburg, D.A., "Geochemistry of natural-gas hydrates in oceanic sediments", Advances in Organic Geochemistry, 1981, 422.

Lapham, L.L., Chanton, J.P., Martens, C.S., Woolsey, J.R., 2008. Microbial activity in surficial sediments overlying acoustic wipe-out zones at a Gulf of Mexico cold seep. Geochemistry, Geophysics, Geosystems 9 (6).

McGee, T., J. R. Woolsey, L. Lapham, R. Kleinberg, L. Macelloni, B. Battista, C. Knapp, S. Caruso, V. Goebel, R. Chapman, P. Gerstoft., 2009. "Structure of a Carbonate/Hydrate Mound in the Northern Gulf of Mexico." Center for Marine Resources and Environmental Technology, University of Mississippi.

Macelloni, Leonardo, A. Simonetti, J. H. Knapp, C. C. Knapp, C. B. Lutken, L. L. Lapham, 2012. "Multiple resolution seismic imaging of a shallow hydrocarbon plumbing system, Woolsey Mound, Northern Gulf of Mexico." *Marine and Petroleum Geology* 1-15. Mississippi Mineral Resources Institute, 111 Brevard Hall, University of Mississippi, University, MS 38677, USA.

Rutherford, Steven R., and Williams, Robert H., 1989. "Amplitude-versus-offset variations in gas sands." *Geophysics*. Vol. 54, No. 6 (June 1989); P. 680-688.

Sassen, R., and Curiale, J. A., 2006. Microbial methane and ethane from gas hydrate nodules of the makassar strait, indonesia, Org. Geochem., 37, 977-980.

Satyavani, N., N. K. Thakur, Uma Shankar, S. I. Reddi, A. R. Sridhar, P. Prasada Rao, K. Sain and Ramesh Khanna, 2003. "Indicators of gas hydrates: Role of velocity and amplitude" National Geophysical Research Institute, Hyderabad, India. *Current Science*, Vol. 85, No. 9, 10 November 2003.

Shuey, R. T. ,1985. "A simplification of the Zoeppritz equations." *Geophysics,* Vol. 50, No. 4 (April 1985); P. 609-614.

Simonetti, A., Knapp, J. H., Knapp, C. C., Sleeper, K., Lutken, C. B., Macelloni, L., in press. "Spatial Distribution of Gas Hydrates from High-Resolution Seismic and Core Data, Woolsey Mound, Northern Gulf of Mexico." *Marine and Petroleum Geology*.

Sloan, E. D. Jr., 1998. "Clathrate hydrates of natural gases", Marcel Dekker Inc., p. 705.

Trehu, A. M., Ruppel, C., Holland, M., Dickens, G., R., Torres, M. E., Collett, T. S., Goldberg, D., Riedel, M., and Schultheiss, P., 2006, Gas Hydrates in Marine Sediments: Lessons from Scientific Ocean Drilling, Oceanography, Vol. 19, No. 4. 124-142.

Van der Waals, J.H. & Platteeuw, J.C. (1959) Clathrate solutions, Adv. Chem. Phys., 2(1).